EUROFUSION WPMST1-PR(16) 14787

D Brida et al.

Determination of the Stochastic Layer Properties Induced by Magnetic Perturbations via Heat Pulse Experiments in ASDEX Upgrade

Preprint of Paper to be submitted for publication in
22nd International Conference on Plasma Surface Interactions
in Controlled Fusion Devices (22nd PSI)

This work has been carried out within the framework of the EUROfusion Consortium and has received funding from the Euratom research and training programme 2014-2018 under grant agreement No 633053. The views and opinions expressed herein do not necessarily reflect those of the European Commission.

Determination of the Stochastic Layer Properties Induced by Magnetic Perturbations via Heat Pulse Experiments at ASDEX Upgrade

D. Brida[a,b,*], T. Lunt[a], M. Wischmeier[a], G. Birkenmeier[a,b], P. Cahyna[c], D. Carralero[a], M. Faitsch[a], Y. Feng[d], B. Kurzan[a], M. Schubert[a], B. Sieglin[a], W. Suttrop[a], E. Wolfrum[a], the ASDEX Upgrade Team[a], and the MST1 Team[1]

[a] *Max-Planck-Institut für Plasmaphysik, Boltzmannstr. 2., D-85748 Garching bei München*
[b] *Physik-Department E28, Technische Universtität München, D-85747 Garching bei München*
[c] *Institute of Plasma Physics CAS, v.v.i. Prague, Czech Republic*
[d] *Max-Planck-Institut für Plasmaphysik, 17491 Greifswald, Germany*

Abstract

A new experimental method was applied in the tokamak ASDEX Upgrade to estimate the stochastic layer width of a deuterium L-mode discharge with externally applied Magnetic Perturbations. The method relies on the deposition of ECRH pulses in the plasma edge while measuring the divertor target heat flux with high temporal resolution IR thermography and Langmuir probes. The experimental results were compared to simulations of the time dependent heat pulse propagation on a constant plasma background with the EMC3-Eirene code package, using an ad-hoc screening model. If no screening was taken into account in the simulations a decrease in the characteristic heat pulse propagation time was observed, which shows that the heat transport is enhanced compared to the screened cases. No such enhancement was found in the experiment, indicating strong screening. In further simulations the effect of screening on the target fluxes was investigated for varying densities. For low densities it was found that screening reduces the strike line splitting strongly, while for higher densities no strong strike line splitting was found, independent of the screening degree. For strongly detached L-mode conditions with MPs experiments at AUG indicate that the lobe structures vanish completely.

Keywords: ASDEX Upgrade, Magnetic Perturbations, Divertor Heat Flux
2010 MSC: 00-01, 99-00

1. Introduction

Future divertor tokamak devices, such as ITER, are foreseen to be operated in a regime of increased confinement, the so called H-mode. However, the H-mode is prone to Edge Localized Modes (ELMs), quasiperiodic bursts of energy and particles from the edge region, which can lead to a severe life time reduction of the Plasma Facing Components (PFCs). By the application of Magnetic Perturbations (MPs), generated by external coils, ELM mitigation [1] and suppression [2] for certain plasma conditions have been achieved in several tokamaks. MP coils create a non-axisymmetric radial magnetic field component which can cause a topological change in the magnetic field. Near the edge a layer of open field lines is created in which field lines connect to the divertor targets. However, various numerical [3] and theoretical [4] studies show that the plasma creates a non-negligible response field. However, evidence of the plasma response field can often only be obtained by indirect measurements. One important response effect is screening of the MP field at rational surfaces in the plasma [4], which reduces the width of the layer of open field lines and hence leads to a reduction of the effective radial transport in the edge. From the edge transport characteristics one can therefore draw conclusions about the screening degree.

This paper is structured as follows: Section 2 gives an introduction to the magnetic topology induced by MPs and discusses the effects of screening. Section 3 introduces briefly the ad-hoc screening model used throughout this study. In Section 4 the experimental setup and results are described and section 5 presents the corresponding EMC3-Eirene simulations. Section 6 discusses divertor heat fluxes with MPs, with and without screening. Section 7 summarizes the results and gives an outlook on future work.

2. Magnetic Field Structure Induced by Magnetic Perturbations

In this section the 3D magnetic topology change induced by the MPs is qualitatively analyzed for an AUG equilibrium with MPs. The equilibrium was calculated with CLISTE [5] and the MP field was calculated by applying Biot-Savart's law, where the exact geometry of the 8 upper and 8 lower saddle coils installed at AUG was taken into account [6].

*Corresponding author
Email address: dominik.brida@ipp.mpg.de (D. Brida)
[1] See http://www.euro-fusionscipub.org/mst1

In Fig. 1a (left) a *Poincaré plot* of the magnetic field without plasma response effects (vacuum approach) is shown. It can be seen that the MPs lead to the creation of magnetic islands at rational surfaces, i.e. surfaces with a safety factor $q = m/n$, where n and m are integer numbers. Sufficiently far inside the confinement region closed surfaces can still be found between the rational surfaces [7], which appear as closed lines in the Poincaré plot. In the edge region a layer with open field lines is created, i.e. these field lines leave the (former) confinement region and eventually hit the targets in finger like structures, so called *lobes*. The onset of this region can be estimated by the condition that the islands of neighboring rational surfaces overlap [8]. Although historically this region is often called *stochastic layer*, it is not uniformly stochastic as will be discussed in the following.

In Fig. 1b (left) a *connection length plot* (or *laminar plot*) of the divertor region at $\phi_0 = 0$ for the above discussed magnetic field is shown. The connection length L_c at a point (R,z) is here defined as the length from the inner to the outer divertor of the field line which crosses the poloidal plane $\phi = \phi_0$ at (R,z). Field lines on unbroken magnetic surfaces or inside magnetic islands have infinite connection length. The region of open field lines can be roughly divided into stochastic regions, with $L_c \geq 1.0$ km, and laminar flux tubes, where $L_c \leq 0.5$ km [9]. In the stochastic regions the field line paths can be described statistically by a diffusive process [10, 8]. This leads effectively to additional radial diffusive particle and energy transport. In the laminar flux tubes L_c is comparable to that of the Scrape-Off Layer (SOL) and the radial transport can be described by convective processes [10]. In these flux tubes a strong particle and energy confinement reduction is anticipated.

The effect of strong screening can be observed in Fig. 1a (right) and Fig. 1b (right). Screening decreases the size of the magnetic islands on rational surfaces and closes the magnetic flux surfaces again. This pushes the region of open field lines further out and it is expected that this leads to an improvement of the confinement compared to the vacuum case.

3. Screening Model

To take into account MP screening effects an ad-hoc model was implemented. A detailed description of this approach can be found in [11] and only a brief summary is given here.

Islands are created due to the radial (i.e. perpendicular to the equilibrium flux surfaces) field component of the MP field $\vec{B}^{MP}$. However instead of the physical field, a description of the model in terms of the normalized radial field $b^{r,MP} = \frac{\vec{B}^{MP}\cdot\nabla\rho_p}{\vec{B}_{eq}\cdot\nabla\phi}$ is best suited. Here ρ_p is the poloidal flux and $\vec{B}^{eq}$ the equilibrium field. On a flux surface $b^{r,MP}$ can be expressed as a Fourier series:

$$b^{r,MP} = \sum_{-\infty}^{\infty} b^{r,MP}_{m,n} \exp^{i(m\theta^* - n\phi)}, \quad (1)$$

where $\theta^* \equiv \phi/q$ is the straight field line poloidal angle. For simplicity only one toroidal mode number $n = n_0$ is considered here. The index n is therefore dropped and rational surfaces with $q = m/n_0$ can be identified by their poloidal mode number m. The physical meaning of the Fourier components of $b^{r,MP}$ is the following: If $b^{r,MP}_m$ is non-zero at the rational surface m, there will appear an island chain on that surface.

The screening model now assumes that at the rational surfaces radially localized screening currents along $\vec{B}^{eq}$ are induced. Mathematically the screening current on a rational surface m can be represented as

$$\vec{j}^m = \Re\left(I^m \delta(q - m/n_0) exp[i(m\theta^* - n_0\phi)] \frac{\vec{B}_{eq}}{\|\vec{B}_{eq}\|} \right), \quad (2)$$

where I^m is a complex constant, which determines the screening strength, $\delta()$ is the delta function and $\Re()$ indicates that only the real part is taken. This current generates a (normalized) radial field component $b^{r,m}$, with a resonant Fourier component $b^{r,m}_m$ on m. I^m is an ad-hoc parameter which was in this study determined by the

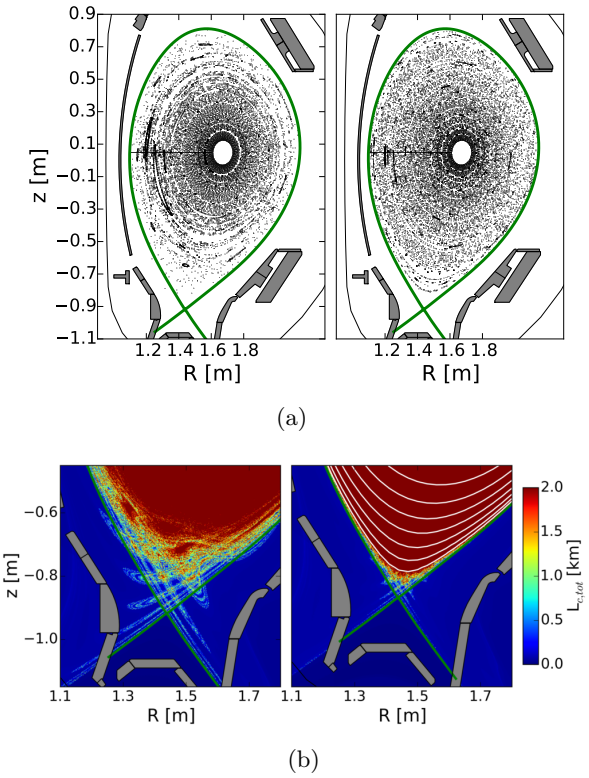

Figure 1: Poincaré (a) and connection length (b) plot at $\phi = 0$ for an equilibrium with MPs without plasma response (left) and with strong screening (right).

condition that the resonant component of the total radial magnetic field vanishes on m. E.g. if screening on only one rational surface m is assumed, I^m is obtained by the following condition:

$$b_m^{r,m} = -b_m^{r,MP} \tag{3}$$

When assuming screening on multiple rational surfaces $(m_1, m_2, ..., m_M)$, it has to be taken into account that each screening current creates resonant field components on the other rational surfaces. I.e. on each surface $m_i, i = 1, ..., M$ following condition has to be satisfied:

$$\sum_{l=1,..,M} b_{m_i}^{r,m_l} = -b_{m_i}^{r,MP}, \tag{4}$$

which constitutes a linear matrix equation which has to be solved for M unknowns. The screening field $\vec{B}^{scr}$ is then given by the sum of the fields created by the individual screening currents

$$\vec{B}^{scr} = \sum_{l=1,..,M} \vec{B}^m \tag{5}$$

and the total magnetic field is calculated as

$$\vec{B} = \vec{B}^{eq} + \vec{B}^{MP} + \vec{B}^{scr}, \tag{6}$$

Numerically the sheet currents were implemented by discretizing them into triangles. The magnetic field generated by the current in each of the triangles can be computed analytically [12]. This approach avoids the problem of a diverging field near the surfaces which occurs when filaments are used for the discretization, as done in [11]. The triangularization for a (3,2) surface is visualized in Fig. 2.

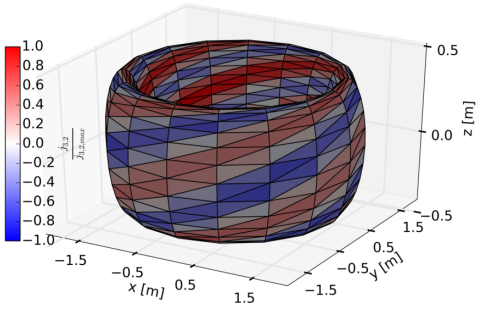

Figure 2: Triangularization of the (3,2) rational surface. For displaying reasons the number of triangles in the plot is lower than actually used in the computations.

4. Experiment

A dedicated L-mode deuterium discharge with a toroidal magnetic field B_t=-2.5 T, plasma current I_p=1.0 MA and safety factor $q_{95} \approx 4.0$ was carried out at AUG. Selected time traces of the discharge can be seen in Fig. 3. The line integrated central electron density was feed-back controlled to $\sim 3.7{\times}10^{19}$ m^{-2} and from 1.2 s on temporally constant central Electron Cyclotron Resonance Heating (ECRH) of $\sim$ 0.4 MW was applied. From 2.3 s on, in addition to the central ECRH heating, ECRH pulses with $\sim$ 0.6 MW were deposited in the edge region. The pulse duration was $\sim$ 2 ms and the period time 26 ms. At 3.7 s the ECRH pulse power was increased to $\sim$ 1.2 MW. From 3.0 to 4.0 s MPs with a toroidal mode number n=2 and a differential phase of $\Delta\phi = 90°$ between upper and lower MP field were applied.

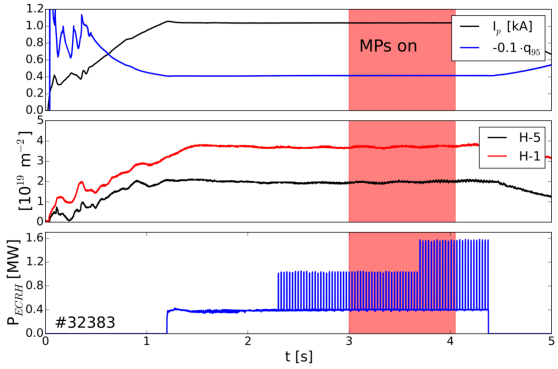

Figure 3: Time traces of AUG discharge 32383.

The outer divertor target was observed at $\phi \approx 214°$ by an infrared camera, measuring the target temperature [13]. The THEODOR code [14] was used to calculate target heat fluxes $q_\perp$ with a temporal resolution of $\sim$ 1 ms and a spatial resolution $\sim$ 0.6 mm. In Fig. 4b the time trace slice between 3.7 s and 4.0 s of the heat flux measurements is shown. It can be clearly seen that each heat pulse leads to a distinct increase of the heat flux. Before the MPs are switched off at 4.05 s so called strike line splitting can be observed. Fig. 4a shows the estimated total heat flux P_{tot} at the outer target after a heat pulse as a function of time t for the MP on and MP off case. Here $P_{tot}(t, \phi) \equiv 2\pi R \int q_\perp(s, \phi, t) ds$, where R is the major radius of the target and conditional averaging over several heat pulse periods was applied. It can be seen that, except for a constant background which was subtracted, P_{tot} coincides for the MP on and off cases within the error bars. The heat pulses could also be observed in the heat flux measured by the outer divertor target triple Langmuir probes at $\phi \approx 168°$ with a time resolution of $\sim$ 35 μs (Fig. 4c). The probe nearest to separatrix measures a decrease of $q_\perp$. This might be attributed to a strike line shift of $\sim$ -0.4 cm during the heat pulse, which can be caused by a current perturbation due to the additional heating.

5. EMC3-Eirene Simulations

The transport of the heat pulse was simulated with a modified version of the 3D transport code EMC3-Eirene

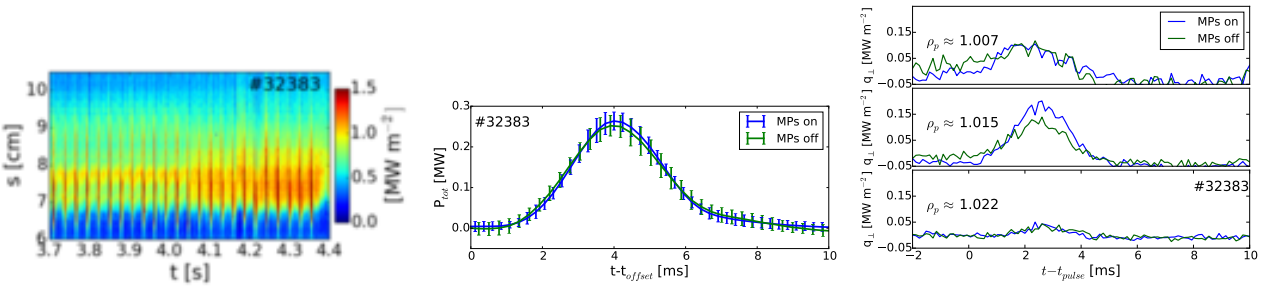

(a) (b) (c)

Figure 4: Outer target heat flux at $\phi \approx 214°$ along the target coordinate s and time t, obtained by the 2D infrared diagnostics (b) and conditionally averaged estimated total heat flux P_{tot}, without background, at the outer target after a heat pulse. Outer divertor heat flux obtained from Langmuir probes at $\phi \approx 168°$ (c). A constant background was subtracted.

[15], which couples the fluid code EMC3 with the kinetic neutral code Eirene. Both, EMC3 as well as Eirene, employ a Monte-Carlo technique to solve the underlying equations. EMC3-Eirene has already been used successfully to simulate the plasma edge transport with MPs in several tokamaks [6, 9, 16]. By comparing the heat transport modelling results for different plasma screening strengths to the experimental results, conclusions about the screening strength in the experiment can be drawn. In addition to the case without MPs (2D), three different plasma response scenarios for the MP-on case were considered: no screening (vacuum), moderate screening and strong screening. For the moderate and strong screening scenarios all rational surfaces within $\rho \leq 0.97$ and $\rho \leq 0.996$ were screened, respectively, by making use of the screening model discussed in section 3.

The heat pulse transport was modeled on a constant plasma background, i.e. for each of the four cases the background plasma was self-consistently simulated, using the same transport coefficients for all four scenarios. The heat pulse transport was then simulated by solving the time dependent energy equation on the constant plasma background.

5.1. Background Plasma

As boundary conditions for the background plasmas a poloidally averaged separatrix density n_{sep}=1.2×10^{19}m^{-3} and a net input power P_{net}=0.4 MW were chosen. For the ad-hoc perpendicular particle diffusion coefficients a spatially constant value $D_\perp$=0.1 m^2 s^{-1} was assumed, while for the ion and electron perpendicular heat diffusion coefficient $\chi_{i,e,\perp}$=0.4 m^2 s^{-1} inside and $\chi_{i,e,\perp}$=0.25 m^2 s^{-1} outside the separatrix were chosen. This values result from matching the 2D solutions to the experimental upstream and target profiles. In Fig. 5 2D cross-sections of the electron temperature T_e and density n_e at the toroidal angle $\phi = 11.25°$ for the 2D case, the vacuum approach case and the moderate screening case are shown. Both, T_e as well as n_e are strongly reduced for the vacuum case compared to the 2D case, while no such reduction is observed for the screened case. In Fig. 6a the MP-off experimental upstream profiles for the electron temperature (top) and density (bottom), obtained by Thomson scattering, and the corresponding simulations profiles at $\phi = 11.25°$ for the four different cases are plotted. While the upstream profiles of the screened cases agree within the experimental error bars with the 2D case, for the vacuum case a reduction of temperature and density of $\sim$ 35 % and $\sim$ 25 %, respectively, is seen at $\rho \approx 0.90$, which is larger than the corresponding error bars. Such a confinement degradation was not observed in the experiment.

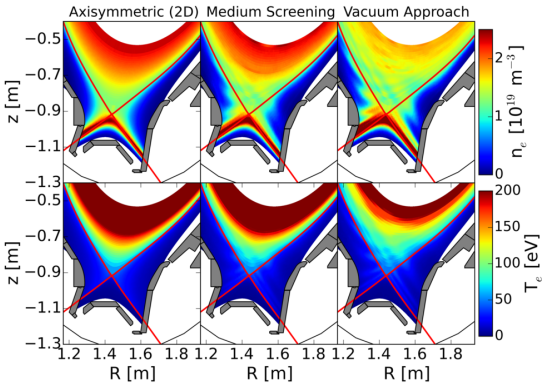

Figure 5: 2D cross-sections of the divertor region at $\phi \approx 11.25°$ of the electron density n_e (top) and temperature T_e (bottom) for the axisymmetric (left), moderately screened (middle) and vacuum (right) case.

In Fig 6b the measured outer target profiles for the MP-off (left) and MP-on (right) cases are shown. To the heat flux profiles, obtained by the IR measurements at $\phi \approx 214°$, a poloidal shift was applied and a constant background of 0.25 MW was subtracted by using the fit function given in [17]. For the 2D case a very good agreement between the simulated heat flux $q_\perp$ and the IR measurements at the outer target was achieved. The experimental ion flux was obtained by the outer target Langmuir probes at $\phi \approx 168°$. The probe profile was shifted along the tar-

get by $\sim$ 1.5 cm, which can be justified by equilibrium errors. In the private flux region and the near SOL a good agreement of $j_\perp$ with the Langmuir probe measurements was achieved, while for s-s$_{sep} > 5cm$ the simulations underestimate the measured j$_\perp$. For the vacuum approach simulation pronounced strike line splitting can be observed in q$_\perp$ as well as in j$_\perp$. With increasing screening the striation pattern becomes less pronounced and the maximum of q$_\perp$ moves nearer to the strike line. In addition the total ion flux decreases.

5.2. Heat Pulse Simulations

To obtain realistic initial conditions for the heat pulse transport simulations the radial deposition profile of the heat pulses were calculated with the beam tracing code TORBEAM [18]. The 'core echo' was neglected in the simulations, i.e. heat which crossed the inner simulation boundary was absorbed. Repeating the simulations with an energy-reflecting inner boundary did not result in significantly different solutions for sufficiently short simulation time ranges, which shows that the results do not depend strongly on the inner simulation boundary conditions. Fig. 7 shows the outer target total heat flux P$_{tot}^{sim}$ as a function of time for the four degrees of screening. Here P$_{tot}^{sim}$ is defined analogously to the experiment. With increasing screening, the heat flux maximum as well as the width decrease. The strong screening case does not differ significantly from the 2D solution. This result indicates that the MP field in the experiment is strongly screened.

Fig. 8 depicts the power flux at three different positions along the target at $\phi \approx 214°$ in dependence of time. As more surfaces are screened, the power at the outer two positions decreases.

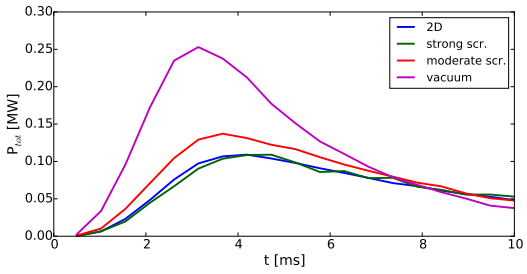

Figure 7: Simulation results of the poloidally integrated outer target heat flux P$_{tot}^{sim}$ at $\phi \approx 214°$ after the heat pulse deposition.

6. Effect of Screening on Target Fluxes and Detachment with MPs

In Fig. 6b it has been seen that strike line splitting is less pronounced when screening currents are present. In this section the effect of screening on strike line splitting for different upstream densities will be analyzed in more detail. For this EMC3-Eirene simulations with P$_{in}$=0.2 MW, D$_\perp$=0.1 m^2 s^{-1} and $\chi_\perp$=0.4 m^2 s^{-1} (typical L-mode parameters) with varying separatrix densities n$_{sep}$ were conducted. A case without screening (vacuum), moderate screening and strong screening were considered. Fig. 9 shows the target heat $q_\perp$ and particle j_{sat} fluxes obtained from the simulations for n$_{sep}$=0.3$\times$10^{19}m^{-3}, n$_{sep}$=0.9$\times$10^{19}m^{-3} and n$_{sep}$=1.5$\times$10^{19}m^{-3}. For the low density case a pronounced strike line splitting in the heat flux profile can be observed for the vacuum case. The strike line splitting gets less pronounced and the peak heat flux increases by $\sim$ 25 % as screening gets stronger. With increasing density the lobes broaden and the effect of screening is less apparent. The washing-out effect of the lobes can be attributed to the decreasing divertor temperature with increasing density, reducing the parallel conductivity and hence increasing the relative effect of perpendicular diffusion [19].

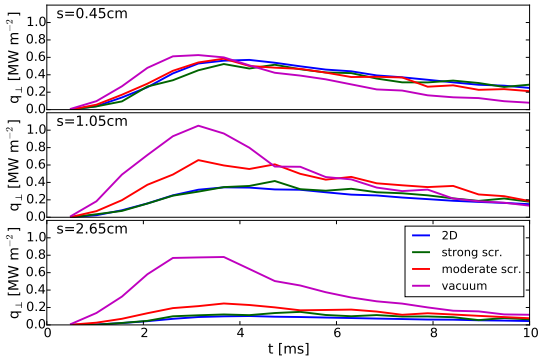

Figure 8: Simulated heat flux after the heat pulse deposition for several target positions at $\phi \approx 214°$.

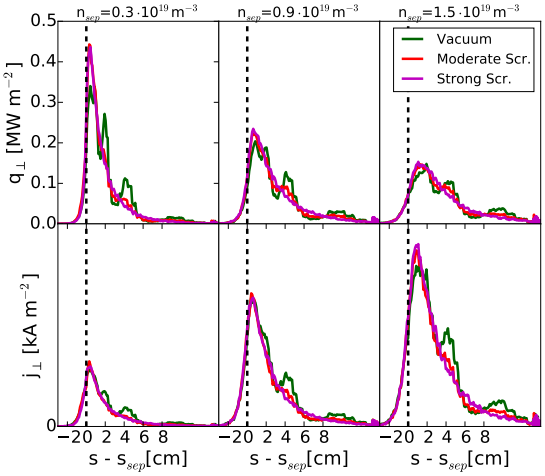

Figure 9: EMC3-simulation results for the outer target heat $q_\perp$ (top) and ion flux $j_\perp$ (bottom) for different averaged seperatrix densities n_{sep} and varying screening degrees.

Of particular interest are divertor fluxes under detached conditions with MPs, since the lobe structure might hin-

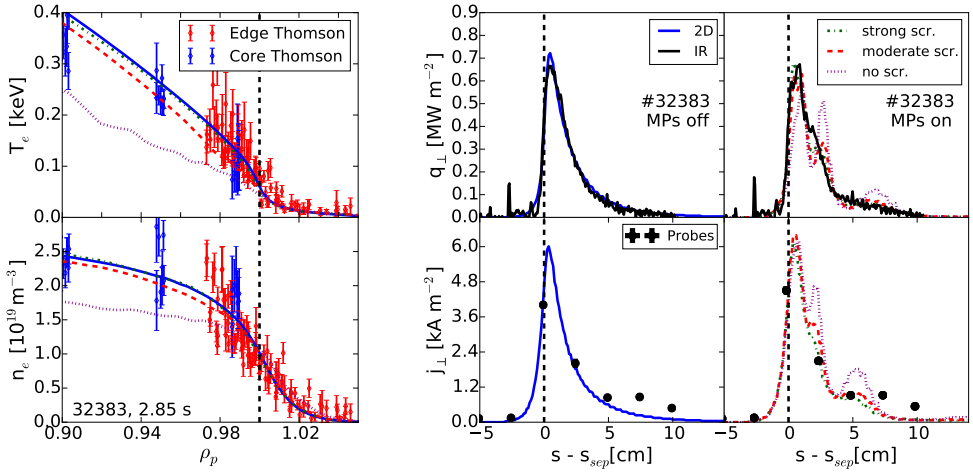

(a) (b)

Figure 6: (a) Upstream profiles for electron density T_e (top) and temperature n_e (bottom). (b) Target profiles for the MP off case (left) and MP on case (right)

der detachment at locations which are at a lobe maximum. At AUG dedicated experiments were carried out in which divertor fluxes with MPs under detached conditions were investigated in detail in L- and H-modes. At these conditions heat flux profiles can only be obtained by the Langmuir probes at AUG, since the IR data is dominated by Bremsstrahlung. In Fig. 10 the power flux obtained by the outer divertor Langmuir probes at $\phi \approx 168°$ of two L-mode density ramps are plotted: 32921 is without MPs and 32922 with n=2 MPs which were rigidly rotated at 5 Hz at $\Delta\phi = -90°$. Due to the toroidal asymmetry of the target fluxes the rigid rotation of the MPs was mandatory to obtain 2D target profiles. In the bottom plot the corresponding deuterium gas puff is shown, which was the same in both discharges. Power detachment starts in both cases at the strikeline and proceeds then outwards towards the far SOL. In the shot with MPs an oscillation of the power flux at the MP rotation frequency is observed, particularly in the signals of the probes located at $\rho \approx 1.01$ and $\rho \approx 1.02$. As stronger detachment sets in these oscillations vanish, i.e. no reattachment occurs. It should be noted at this point that EMC3-Eirene does not yet include recombination processes and therefore detached conditions could not be simulated.

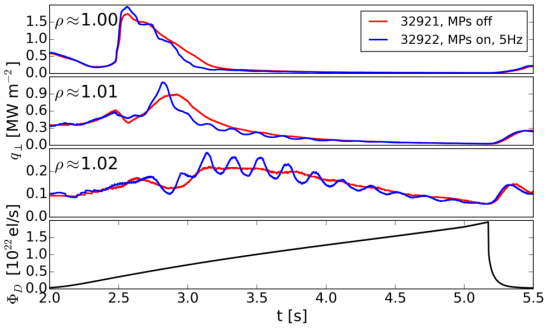

Figure 10: Langmuir probe heat flux $q_\perp$ for the L-mode density ramps 32921 (red) without MPs and 32922 (blue) with n=2, $\Delta\phi = -90°$, at 5 Hz rigidly rotating MPs, and the corresponding deuterium gas puff level Φ_D.

7. Conclusions

A new experimental approach to determine the stochastic layer width of a magnetically perturbed plasma was introduced, which relies on the increased energy transport in a stochastized field. An L-mode experiment at AUG was carried out in which ECRH heat pulses were deposited at the edge. The heat pulses led to an increased heat flux at the outer target, which was observed by various divertor diagnostics. The temporal characteristics of the power flux did not show any significant difference when MPs were switched on and off. The result was interpreted by comparison with EMC3-Eirene simulations, where an ad-hoc screening model was used. Assuming screening of rational surfaces with $\rho < 0.996$ the experimental result could be qualitatively reproduced, indicating that strong screening occurs.

The effect of screening on the target fluxes for different upstream densities was investigated with EMC3-Eirene. For low densities screening leads to a strong reduction of the strike line splitting in the power flux. With increasing density the lobes get washed-out and no significant difference in the power flux for different screening degrees was found. Experiments at AUG show that the lobe structures vanish in detached conditions.

8. Acknowledgments

This work has been carried out within the framework of the EUROfusion Consortium and has received funding from the Euratom research and training programme 2014 - 2018 under grant agreement No 633053. The views and opinions expressed herein do not necessarily reflect those of the European Commission.

References

[1] W. Suttrop, Phys. Rev. Lett. 106 (2011) 225004. doi:10.1103/PhysRevLett.106.225004.

[2] T. Evans, M. Fenstermacher, R. Moyer, T. Osborne, J. Watkins, P. Gohil, I. Joseph, M. Schaffer, L. Baylor, M. Bcoulet, J. Boedo, K. Burrell, J. deGrassie, K. Finken, T. Jernigan, M. Jakubowski, C. Lasnier, M. Lehnen, A. Leonard, J. Lonnroth, E. Nardon, V. Parail, O. Schmitz, B. Unterberg, W. West, Rmp elm suppression in diii-d plasmas with iter similar shapes and collisionalities, Nuclear Fusion 48 (2) (2008) 024002.
URL http://stacks.iop.org/0029-5515/48/i=2/a=024002

[3] M. Becoulet, F. Orain, P. Maget, N. Mellet, X. Garbet, E. Nardon, G. Huysmans, T. Casper, A. Loarte, P. Cahyna, A. Smolyakov, F. Waelbroeck, M. Schaffer, T. Evans, Y. Liang, O. Schmitz, M. Beurskens, V. Rozhansky, E. Kaveeva, Screening of resonant magnetic perturbations by flows in tokamaks, Nuclear Fusion 52 (5) (2012) 054003.
URL http://stacks.iop.org/0029-5515/52/i=5/a=054003

[4] R. Fitzpatrick, Nuclear Fusion 33 (7) (1993) 1049.

[5] P. J. McCarthy, P. Martin, W. Schneider, The cliste interpretive equilibrium code.

[6] T. Lunt, Y. Feng, M. Bernert, A. Herrmann, P. de Marn, R. McDermott, H. Mller, S. Potzel, T. Ptterich, S. Rathgeber, W. Suttrop, E. Viezzer, E. Wolfrum, M. Willensdorfer, the ASDEX Upgrade team, First emc3-eirene simulations of the impact of the edge magnetic perturbations at asdex upgrade compared with the experiment, Nuclear Fusion 52 (5) (2012) 054013.
URL http://stacks.iop.org/0029-5515/52/i=5/a=054013

[7] S. Abdullaev, Magnetic Stochasticity in Magnetically Confined Fusion Plasmas: Chaos of Field Lines and Charged Particle Dynamics, Springer Series on Atomic, Optical, and Plasma Physics, Springer International Publishing, 2013.
URL https://books.google.de/books?id=0vu8BAAAQBAJ

[8] P. Ghendrih, A. Grosman, H. Capes, Theoretical and experimental investigations of stochastic boundaries in tokamaks, Plasma Physics and Controlled Fusion 38 (10) (1996) 1653.
URL http://stacks.iop.org/0741-3335/38/i=10/a=002

[9] O. Schmitz, T. E. Evans, M. E. Fenstermacher, H. Frerichs, M. W. Jakubowski, M. J. Schaffer, A. Wingen, W. P. West, N. H. Brooks, K. H. Burrell, J. S. deGrassie, Y. Feng, K. H. Finken, P. Gohil, M. Groth, I. Joseph, C. J. Lasnier, M. Lehnen, A. W. Leonard, S. Mordijck, R. A. Moyer, A. Nicolai, T. H. Osborne, D. Reiter, U. Samm, K. H. Spatschek, H. Stoschus, B. Unterberg, E. A. Unterberg, J. G. Watkins, R. Wolf, the DIII-D, T. Teams, Aspects of three dimensional transport for elm control experiments in iter-similar shape plasmas at low collisionality in diii-d, Plasma Physics and Controlled Fusion 50 (12) (2008) 124029.
URL http://stacks.iop.org/0741-3335/50/i=12/a=124029

[10] S. Abdullaev, M. Jakubowski, M. Lehnen, O. Schmitz, B. Unterberg, On description of magnetic stochasticity in poloidal divertor tokamaks, Physics of Plasmas (1994-present) 15 (4) (2008) 042508.

[11] P. Cahyna, Journal of Nuclear Materials 415 (1, Supplement) (2011) S927 – S931. doi:http://dx.doi.org/10.1016/j.jnucmat.2011.01.117.

[12] P. Merkel, E. Strumberger, Linear mhd stability studies with the starwall code, arXiv preprint arXiv:1508.04911.

[13] B. Sieglin, M. Faitsch, A. Herrmann, B. Brucker, T. Eich, L. Kammerloher, S. Martinov, Real time capable infrared thermography for asdex upgrade, Review of Scientific Instruments 86 (11) (2015) 113502.

[14] A. Herrmann, W. Junker, K. Gunther, S. Bosch, M. Kaufmann, J. Neuhauser, G. Pautasso, T. Richter, R. Schneider, Energy flux to the asdex-upgrade diverter plates determined by thermography and calorimetry, Plasma Physics and Controlled Fusion 37 (1) (1995) 17.
URL http://stacks.iop.org/0741-3335/37/i=1/a=002

[15] Y. Feng, Contributions to Plasma Physics 44 (1-3) (2004) 25–30. doi:10.1002/ctpp.200410003.

[16] H. Frerichs, O. Schmitz, T. Evans, Y. Feng, D. Reiter, The pattern of parallel edge plasma flows due to pressure gradients, recycling, and resonant magnetic perturbations in diii-d, Physics of Plasmas (1994-present) 22 (7) (2015) 072508.

[17] T. Eich, B. Sieglin, A. Scarabosio, W. Fundamenski, R. J. Goldston, A. Herrmann, Inter-elm power decay length for jet and asdex upgrade: Measurement and comparison with heuristic drift-based model, Phys. Rev. Lett. 107 (2011) 215001. doi:10.1103/PhysRevLett.107.215001.
URL http://link.aps.org/doi/10.1103/PhysRevLett.107.215001

[18] E. Poli, Computer Physics Communications 136 (12) (2001) 90 – 104. doi:http://dx.doi.org/10.1016/S0010-4655(01)00146-1.

[19] B. Sieglin, T. Eich, M. Faitsch, A. Herrmann, A. Scarabosio, the ASDEX Upgrade Team, Investigation of scrape-off layer and divertor heat transport in asdex upgrade l-mode, Plasma Physics and Controlled Fusion 58 (5) (2016) 055015.
URL http://stacks.iop.org/0741-3335/58/i=5/a=055015